Korean J. Chem. Eng., **18**(6), 802-808 (2001)

Experimental Studies on the Flow of Two Immiscible Fluids in Porous Media Using X-ray Computed Tomography: The Case When the Viscosities of the Fluids are Equal

Kyung-Hoe Kim† and Chan-Hong Chung

Department of Chemical Engineering,
Taegu University, Kyungsan, Kyungbuk 712-714, Korea
(*Received 22 December 2000 • accepted 24 July 2001*)

Abstract—Experiments were carried out to demonstrate the dispersion that occurs at the interface between fluids when two immiscible fluids flow in porous structures. In this work the porous medium was cellulosic absorbent and the fluids, decyl alcohol and water, were modified so as to cover a range of flow rates and identical fluid viscosities. Computerized Tomography (CT) was used to generate dynamic three-dimensional images of two-phase saturations and provided quantitative information of time evolution of fluid saturation at each position. Thus, use of CT made characterization of two-phase displacement history in cellulosic porous media possible. This work could relate experimental fluid saturation to theoretical model of immiscible fluids flow.

Key words: Fluid Saturations, X-Ray Computed Tomography, Voxel (Volume Element), Gray Scale Image, Dispersion Coefficient

INTRODUCTION

The flow of immiscible fluid phases in porous media is involved in many displacement processes, such as oil recovery, groundwater contamination, and dispersion of toxic chemicals in soil. The time history of the intramedia spatial saturation distribution of each phase is essential for describing the storage and transport of fluids in porous media.

In general, when two-phase immiscible fluids are flowing in porous media, unstable flow (viscous fingering) may result due to the regime where one fluid is less viscous than the other. The criteria on fluid instability result from viscosity, interfacial tension and properties of media. The displacement of immiscible fluids is of importance in many processes as mentioned above. In those areas, an understanding of the relevant mechanisms is essential for the storage and the transport of fluids in porous media. Three different approaches [Chuoke et al., 1959; Willemsen, 1983; Paterson, 1984] are given to describe the mechanisms linked to the displacement of two immiscible fluids. Unlike previous theoretical approaches, the former paper [Kim and Chung, 2001] is based on a stochastic model. In this model a porous medium is considered to be equivalent to a network of uniform capillaries and flow occurs within a random microscopic capillary network. The former paper is chiefly concerned with the dynamic fluid behavior that takes place in a porous medium. An analytical expression is developed and can describe fluid saturation distribution that agrees qualitatively with that seen in experiment. Such saturation distributions in optically dense media are difficult to acquire because of the inaccessibility to conventional measurement probes.

Several methods have been used, however, for studying fluid saturation distributions during fluid displacement processes. Microwave absorption [Parson, 1975] and resistivity measurement [Leverette, 1939] provide area-average fluid saturation. Transparent porous models [Van Meurs, 1957] show the motion of the fluid interface, even though they do not give quantitative data. Recently, radioisotope tracing by Gamma Camera [Castellana et al., 1980; Huang, 1986] gives two-dimensional projections of the fluid saturation distribution. None of these methods provides the detailed information required for a conclusive study of an immiscible fluids displacement process. In comparison to these traditional techniques, X-ray Computed Tomography (we call this CT hereafter) is a fast and accurate technique which can offer unprecedented information about fluid saturation distributions in porous media during displacement processes, as well as information about rock structures corresponding to local regions within porous media. Wang and coworkers [1983, 1984] were the first to apply medical X-ray tomography to study fluid motion in oil recovery research. Wellington and Vinegar [1985] of Shell reviewed three-dimensional measurement of rock density, porosity, its relevance to rock mechanics, correlation of core logs with well logs, and other petrophysical applications. Flannery et al. [1987] have reported on micro X-ray CT for imaging individual pores with a pixel size of 2.5 μm. More recently magnetic resonance imaging [Vinegar, 1986; Chen et al., 1993] has been used to study flow behavior in a porous medium. Among the fluid flow problems that can be studied with CT are two-phase relative permeability, dispersion, viscous fingering, trapped oil saturation, and imbibition. Computerized Tomography can generate dynamic three-dimensional images of two-phase saturations and provides quantitative information of time evolution of fluid saturation at each position. Thus, the use of CT makes characterization of two-phase displacement history in optically dense porous media possible. This work relates fluid saturation data to the one-dimensional model of immiscible fluids flow developed in the former paper

†To whom correspondence should be addressed.
E-mail: khk9509@taegu.ac.kr

[Kim and Chung, 2001].

EXPERIMENTAL METHOD

1. X-ray Computed Tomography

An EMI CT 5005 transverse axial tomography system used for the experiment is a second-generation scanner (EMI Medical Limited, Slough, U.K.). A tomographic section, nominally 8×10^{-3} m thick, is scanned by using X-rays and the resulting picture is displaced on a video monitor. The system covers the full range of X-ray absorption coefficients of materials normally found in the human body. The range which is linear, extends on an EMI scale where water is zero and air and bone are –500 and +500, respectively. EMI number is defined as

$$500\times\frac{\mu-\mu_{water}}{\mu_{water}} \tag{1}$$

where μ and μ_{water} are linear attenuation coefficient and attenuation coefficient of water, respectively. A scan field of 0.254 m×0.254 m is divided into a 320×320 matrix of picture elements (pixels) of 0.75×10^{-3} m by 0.75×10^{-3} m. The X-ray tube is usually operated at 120 KeV and 30 mA and the detector assembly is comprised of 30 detectors, each combining a doped sodium iodide scintillation crystal photomultiplier. The EMI scanner software performs automatic scan sequence control, concurrent data acquisition, image display and annotation and automatic transfer to a magnetic tape. These CT-generated magnetic tapes were then transferred to a microcomputer where the fluid saturations were computed.

2. The Preparation of Porous Medium Assembly

A quasi-one dimensional porous medium was constructed from 32 sheets of Whatman Number 5 filter paper. Round filter papers (diameter=0.24 m) were cut into rectangular shapes (0.21×0.05 m) and silicone rubber adhesive was evenly applied to four edges. The filter papers were placed together so that the thickness of resulting porous medium was approximately 0.00592 m.

The whole assembly was put in a vacuum oven (21 mmHg) for 20 minutes so that silicone seal developed some degree of cure. The porous medium was then removed from the vacuum oven and put between steel plates having the dimension of 0.21×0.05×0.0048 m. A 4,540 kg force by press (Pasadena Hydraulics Inc., El Monte, CA.) was applied for 24 hours to fully cure the silicone rubber seal. Rubber gaskets were also fixed on the four edges of the fully cured porous medium (0.21×0.05×0.0048 m) to prevent leakage of fluid during the displacement experiments. The porous medium having the rubber gaskets was then siliconed to PVC plate and assembled to keep the gap of 0.0048 m. The silicone rubber was completely cured for 24 hours to secure the leakage of fluid.

The PVC plate was mounted on a positioning jig on the CT machine and it was scanned in the dry state to assume structural uniformity. The uniform distribution of X-ray attenuation coefficient with respect to distance proved that the cellulosic bed consisted of a homogeneous porous structure. The porosity of cellulosic bed determined by experiment is to be 0.7. It is assumed that the void fraction of each porous media is constant and independent of fluid occupying it.

3. Fluid-Displacement Experiments

The prerequisites for fluids used in displacement experiments are: (1) There must be immiscibility between displaced fluids and displacing fluids. (2) The contact angle of the liquids with cellulose must be near 90 degrees so as to minimize capillarity. The immiscible fluids used were water containing 47.6 wt% sucrose (displacing fluid) and decyl alcohol (displaced fluid). CT experiments only differentiate between fluids if displacing fluid has higher attenuation than displaced fluid. 47.6 wt% sucrose solution was tagged with 0.4 M KI solution to increase its X-ray attenuation coefficient. This concentration gave optimal contrast with decyl alcohol and minimized beam hardening.

When 47.6 wt% sucrose solution (viscosity=13.63 cP at 21.5°C) displaced decyl alcohol (viscosity=13.45 cP at 21.5°C) saturated in pore structure, viscosity difference between two fluids was 0.18 cP (we call this case zero viscosity difference hereafter). The viscosity of water was modified by sucrose. Decyl alcohol was selected as displaced fluid because its viscosity was equivalent to sucrose solution and had a near neutral wettability to cellulose. Decyl alcohol is also immiscible with water.

Fig. 1 shows the CT experimental layout. Displacement experiments were carried out by mounting cellulosic porous medium between two circular plates of poly(vinyl chloride) shown in Fig. 2. For assembling of the porous bed care was taken to ensure that the gap between two plates was maintained constant by using polyethylene spacers. Nylon bolts (transparent to X-ray) secured these plates. Positioning arrangement was used to place absorbent mounting frame exactly within the tomographic plane of the CT scanner. After the absorbent mounting frame was centered in the CT scanner, dry cellulosic porous medium was first scanned to ensure the homogeneity of porous structure inside the bed. Ten pore volumes of dis-

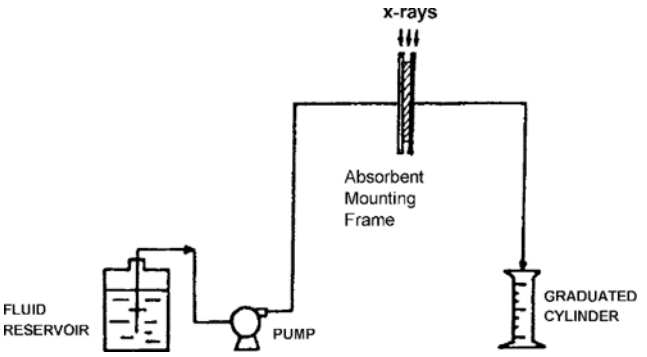

Fig. 1. Schematic diagram of experimental setup.

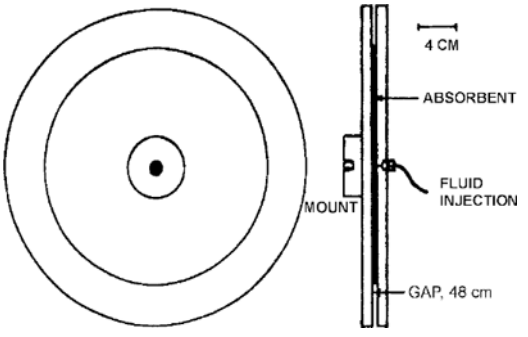

Fig. 2. Absorbent mounting frame of poly(vinyl chloride) (dimension in cm).

placed fluids were injected to saturate the porous medium after evacuation. Uniform saturation of porous medium was confirmed by CT image before displacement experiment. A displacing fluid was injected at 3 flow rates, such as 0.137 cm^3/min, 1.02 cm^3/min, and 4.04 cm^3/min. The image data were taken at every 30 seconds during displacement experiments. Eight image data were selected from each flow rate to confirm theory. The local X-ray attenuation coefficient was recorded for each pixel position of the image. All volumetric flows were verified by monitoring the volume of fluid in a graduated cylinder. Adjusting the height of outlet tube relieved gravity effect. For the conversion of CT data into saturation fraction (displacing/displaced fluid composition), the attenuation coefficient distributions to fluids were determined over a cross-section of cellulosic porous bed. The magnitude of the minor fluctuations in the CT data was measured and compared to the expected CT scanner noise and/or porosity variation.

DATA REDUCTION

A two-phase displacement experiment requires two kinds of reference image data in order to compute the saturation fraction. One is taken from the cellulosic porous medium saturated only with displacing fluid and the other with only displaced fluid. The linear attenuation coefficient of a specific voxel (volume element) (i, j) (Fig. 3), $\mu_{i,j}$, is a linear combination of the attenuation coefficients of all existing components

$$\mu_{i,j}=(1-\phi_{i,j})\,\mu_{cellulose}+\phi_{i,j}\mu_{1\text{ or }2} \tag{2}$$

where $\phi_{i,j}$ is the void fraction of the volume element (i, j), $\mu_{1\text{ or }2}$ stands for the attenuation coefficient of the displacing fluid (subscript 1) or displaced fluid (subscript 2). When each porous medium is saturated with the displacing and displaced fluid respectively, the attenuation coefficients for the voxel (i, j) are,

$$\mu_{1,cellulose}=(1-\phi_{i,j})\mu_{cellulose}+\phi_{i,j}\mu_1 \tag{3}$$

$$\mu_{2,cellulose}=(1-\phi_{i,j})\mu_{cellulose}+\phi_{i,j}\mu_2 \tag{4}$$

The attenuation coefficient for the same voxel when the porous medium now contains both fluids is,

$$\mu_{i,j}=(1-\phi_{i,j})\mu_{cellulose}+\phi_{i,j}x_{i,j}\mu_1+\phi_{i,j}(1-x_{i,j})\mu_2 \tag{5}$$

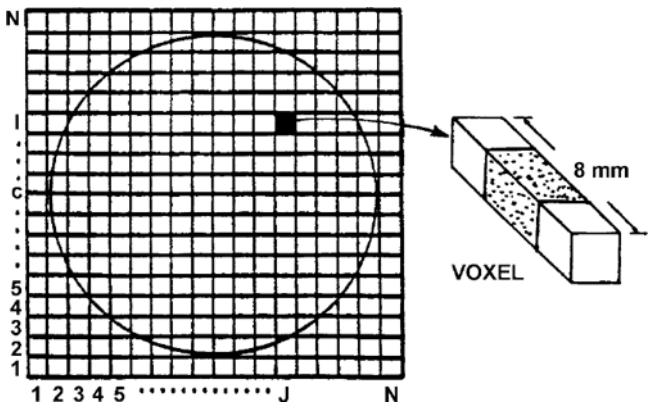

Fig. 3. A voxel (i, j) of whole object consists of cellulosic absorbent in center and plastic plates in both sides.

Combining the above equations, an equation for the saturation of the displacing fluid is obtained,

$$x_{i,j}=\frac{\mu_{i,j}-\mu_{2,cellulose}}{\mu_{1,cellulose}-\mu_{2,cellulose}} \tag{6}$$

Eq. (6) is the fundamental relationship that links the attenuation coefficients to fluid saturations. To calculate the saturation fraction accurately, the attenuation coefficient distribution of $\mu_{1,cellulose}$ and $\mu_{2,cellulose}$ was checked over the cross-section of the porous medium. The effect of beam hardening (the increase of X-ray average energy during the passage through the material that results from the larger attenuation of the lower energy part of the beam) was shown to be negligible. From the difference between $\mu_{1,cellulose}$ and $\mu_{2,cellulose}$ and the precision in which these numbers can be obtained, it is shown that the fluid saturation can be obtained within about ±1.5% error range. Experimental results showed a pronounced variation of X-ray attenuation numbers along the direction of overall displacement and negligible variations in other directions. Therefore, flow took place mainly in one direction and the saturations were computed by taking the average X-ray numbers of the central 15 pixels region.

In the following paragraphs the steps taken to reduce image data to physical dispersion coefficients are discussed. These steps include estimating local fluids saturation along the position of flow direction, differentiating saturation-distance data and extracting $P^{(1)}(x, t)=-\partial\Phi_{II}/\partial x=\rho^{(1)}(x, t)/M$ (we express this term as $P^{(1)}$ hereafter) along the position axis [see Eq. (26); Kim and Chung, 2001]. In the simplest interpretation, the average displacement rate β and the dispersion constant D can be determined from the first moment and second moment of the distribution of $P^{(1)}$ along the position axis. The first moment is defined by:

$$\langle x\rangle=\frac{\int_0^\infty xP^{(1)}dx}{\int_0^\infty P^{(1)}dx} \tag{7}$$

also we have,

$$\langle x\rangle=\beta t \tag{8}$$

in which β is the average displacement rate and is easily determined from <x> and optimal time.

The second moment is defined by:

$$\langle x^2\rangle=\frac{\int_0^\infty x^2P^{(1)}dx}{\int_0^\infty P^{(1)}dx} \tag{9}$$

A dispersion coefficient D can be computed by;

$$\langle x^2\rangle-\langle x\rangle^2=2Dt \tag{10}$$

EXPERIMENTAL RESULTS AND DISCUSSIONS

The liquid-liquid contact angle (taken through water) was measured on cellophane film and found to be 83 degrees. Thus, all experiments were designed so that capillarity effects would be minimal. Viscosity differences and fluid displacement rates would be the principal variables.

Average EMI number of decyl alcohol saturated cellulosic bed and sucrose solution saturated bed were shown as 68.4 and 398.3,

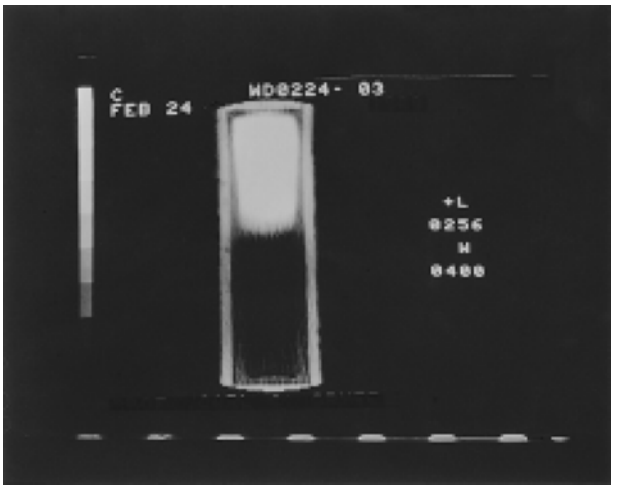

Fig. 4. Gray scale image of sucrose solution (0.4 M KI doped) displacing decyl alcohol at the flow rate of 1.02 cm³/min (white area means sucrose solution).

respectively. The difference between decyl alcohol and sucrose data (EMI 329.9) is proportional to the fraction of decyl alcohol in the porous structure. Local fluid saturation along the position can be accurately estimated by using the calibration data and Eq. (6).

1. Gray Scale Images

In Fig. 4 a gray scale image of CT was given for experiment in which sucrose solution displaced decyl alcohol for the flow rate of 1.02 [cm³/min]. This is typical of all image data used in displacement experiments. It is seen that the interface between displaced and displacing fluid is flat and that there is very little tendency for a fluid projection (or finger to form). Thus, the central 15 pixels section in flow direction can be fully representative of the displacement experiment.

2. Displacing Fluid Saturations as a Function of Position

Figs. 5(a)-5(c) show displacing fluid saturation fraction as a function of position at different time with increasing fluid displacement rate. Distance is measured in pixels, each pixel being 0.75 mm wide. These figures are the fundamental plots out of which dispersion coefficients can be ultimately estimated. Increasing displacement rate broadens the saturation zone of displacing fluid. For a given displacement rate, particularly in Fig. 5(c), it is evident that at longer times the broadening of the zone occurs between displacing and displaced fluid. It is also observed that the displacing fluid does not even at very large time displace all of the displaced fluid from the porous media. This residual saturation is observed in Fig. 5(a)-5(c) to be 0.11 saturation fraction and is independent of displacement rate.

3. Fractional Concentration of Microscopic Interfaces at a Position x

Eq. (11) [the same equation as Eq. (28); Kim and Chung, 2001] defined $\rho^{(1)}(x, t)$ as the concentration of microscopic interfaces. $P^{(1)}$ can be determined directly from experimental data. Since $P^{(1)}$ is defined as $P^{(1)}=-\partial\Phi_{\#}/\partial x$ at t, then the slopes in Fig. 5 give $P^{(1)}$ as a function of position.

$$\rho^{(1)}(x,t)=\frac{M}{(4\pi Dt)^{1/2}}\exp-\frac{(x+\beta t)^2}{4Dt} \qquad (11)$$

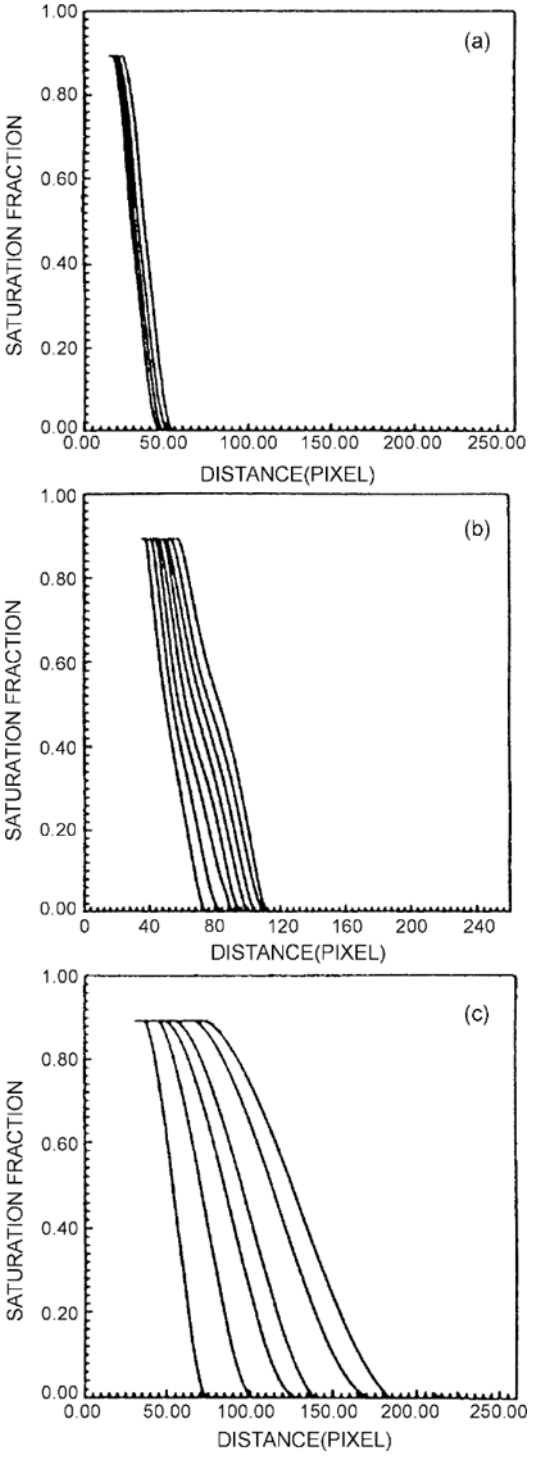

Fig. 5. The variation of saturation fraction along with distance at different time interval (in case of zero viscosity difference) (a) 0.137 cm³/min (b) 1.02 cm³/min (c) 4.04 cm³/min.

Since a complete theoretical description exists for the case of viscosity difference equal to zero [Kim and Chung, 2001], the spatial variation of $P^{(1)}$ can also be determined. In Fig. 6(a)-(c), the fractional concentration of microscopic interfaces, $P^{(1)}$ has been plotted as a function of position for the three different flow rates. $P^{(1)}$ is an indication of the spatial distribution of the fraction of microscopic

interfaces. The width of this distribution, which looks gaussian, depends on time and is a measure of the underlying spreading phenomena associated with the random walking of the individual microscopic interfaces.

4. Calculation of Average Displacement Rate

The average displacement rate, β can be determined from the data in a number of ways. Through these determinations one can check the experimental results for internal consistency. The experimental flow rate Q was measured in each experiment and held constant. However, the data shown do not reflect the complete area of displacement (e.g., the edge regions are not included) and thus the experimental Q does not always exactly apply.

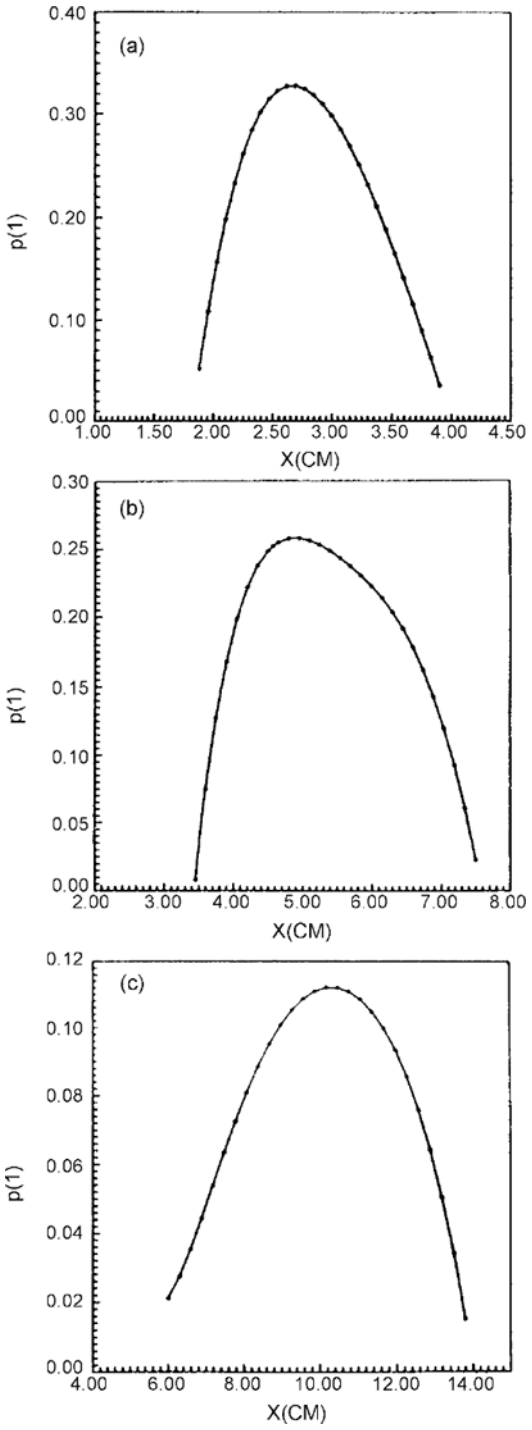

Fig. 6. Fractional concentration of microscopic interfaces as a function of distance (in case of zero viscosity difference) (a) 0.137 cm³/min, t=26 min (b) 1.02 cm³/min, t=9 min (c) 4.04 cm³/min, t=4.5 min.

Table 1. Average displacement rate, $\beta \times 10^2$ [cm/sec]

Method	Experimental flow rate, Q		
	0.137 [cm³/min]	1.02 [cm³/min]	4.04 [cm³/min]
From integration of $P^{(1)}$ - position plots	0.17	1.0	4.0
From Q/effective area	0.19	1.4	5.0

The average displacement rate can be determined most appropriately from $P^{(1)}$ - position plot (Fig. 6). The quantity β is given first moment method by Eq. (7) and Eq. (8). For each of the Fig. 6 this integral has been determined and β values are given in Table 1.

There is a difference between β derived from experimental Q and β derived from $P^{(1)}$ - position plots. For the case of high flow rate experiments where pressure gradient is the greatest, irregularities in the flow (at the edges for example) account for this discrepancy.

5. Determination of Dispersion Coefficients

Eq. (11) forms the theoretical basis for the relationship among $\rho^{(1)}(x, t)$, the concentration of microscopic interfaces, position and time. For the case of equal viscosities, a dispersion coefficient may be unambiguously deduced from the experimental data. Using $P^{(1)}$ - position plots as shown in Fig. 6, dispersion coefficient, D can be determined from a second moment method by Eq. (9) and Eq. (10) for three different flow rates. These data together with experimental flow rates are given Table 2.

Using experimentally determined parameters (β and D) and using Eq. (12) [the same equation as Eq. (31): Kim and Chung, 2001], theoretical curves of fluid saturation were generated as a function of time and position for three different flow rates.

$$\Phi_{ij} = \frac{1}{2}\mathrm{erfc}\left(\frac{x+\beta t}{2\sqrt{Dt}}\right) \tag{12}$$

These theoretically derived curves were then superimposed over the experimental data points in Fig. 7. Points indicate experimental data, while the solid line represents Eq. (12). At flow rate of 0.137 [cm³/min], there was good agreement between the experimental and theoretical results. The fitted average dispersion coefficient ($D = 1.43 \times 10^{-4}$) fits the experimental data adequately at these displace-

Table 2. The comparison of dispersion coefficients by data analysis with those by theoretical curve fitting, D [cm²/sec]

Method	Experimental flow rate, Q		
	0.137 [cm³/min]	1.02 [cm³/min]	4.04 [cm³/min]
From data analysis of $P^{(1)}$ - position plots	1.44×10^{-4}	1.07×10^{-3}	5.47×10^{-3}
From theoretical curve fitting	1.43×10^{-4}	1.01×10^{-3}	5.2×10^{-3}

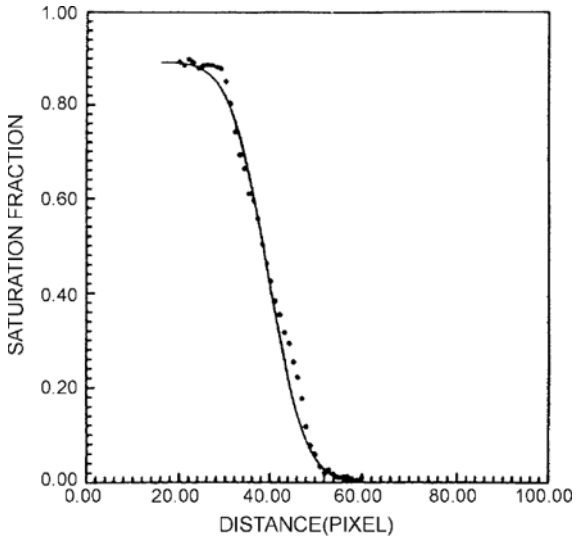

Fig. 7. The comparison of experimental data points with theoretically derived curve at the flow rate of 0.137 cm³/min.

ment rates. The same dispersion coefficient was used over a considerable range of displacement and time. For experimental range of flow rate, all the data are well described in terms of a constant dispersion coefficient and thus an effort was made to quantify the closeness of the fit between data and theory. The variance was checked at the different times for three flow rates considered. At flow rate of 0.137 [cm³/min] the variance after the injection of 3.27 cm³ of fluid (first data set) was about the same as after the injection of 4.62 cm³ of fluid (eighth data set). Also, the variances at higher flow rates were somewhat higher but in the same range and had the same constancy with degree of displacement. These were general observations in all experimental ranges of flow rate. The fitted average dispersion coefficients are reported in Table 2 for the three flow experiments. A Fickian dispersion coefficient is, therefore, appropriate for the description of immiscible displacement in a random porous media.

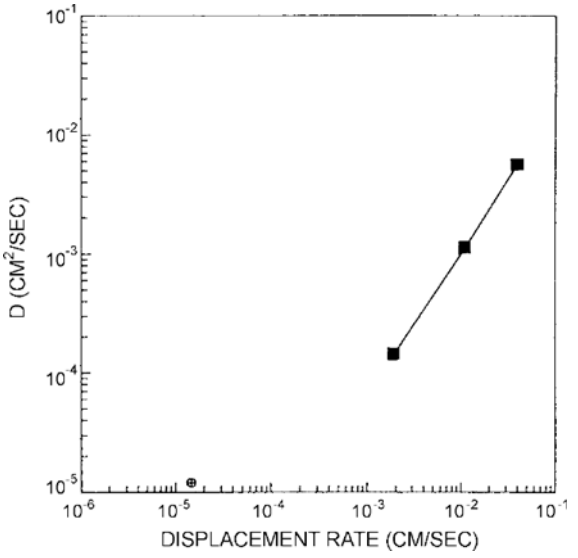

Fig. 8. Dispersion coefficient versus displacement rate.

6. Dispersion Coefficient as a Function of Displacement Rate

Fig. 8 shows dispersion coefficient D as a function of displacement rate β. The relationship as predicted by theory is linear.

$$D = \frac{Qp l_p}{2\pi r_c^2} \tag{13}$$

The value of dispersion coefficient can be used to calculate the length of a jump or segment. It is known that the void fraction can be expressed as,

$$\phi = \frac{\pi r_c^2 M}{(1-\text{residual saturation})A} \tag{14}$$

Eliminating M and r_c from Eq. (14) by using Eq. (13),

$$D = \frac{Q l_p}{2\phi(1-\text{residual saturation})A} \tag{15}$$

The length of a jump can thus be calculated from the above equation. Flows measurements and Darcy's law predict that r_c is of the order of 20 microns, which is also confirmed by SEM photomicrograph (Fig. 9). This gives M/A to be about 50,000 per unit area of porous bed. The value of l_p obtained was 1.300×10^{-3} m. At first glance this jump length appears to be too high. This is the result of the assumption that restricts all of the porous domains of the paper to capillaries existing in a single direction. It is much more reasonable to assume that the pore volume is isotropic in all coordinate directions. Since motion is restricted to one direction there will be a jump only in the flow direction x. The pores in the directions perpendicular to the flow direction appear as dead end pores, occupy volume but do not advance the interface. The residual trapped volume is part of these pores. If this is true then the length of segment should be 4.33×10^{-4} m. The value appears to be of reasonable dimension providing suitable microscopic steps of sufficient frequency so that a statistical approach to the displacement phenomena appears warranted.

CONCLUSIONS

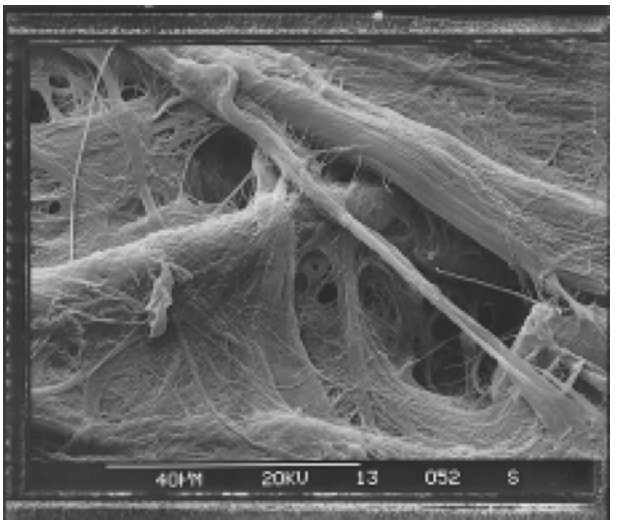

Fig. 9. Scanning electron photomicrograph of Whatman number 5 filter paper.

Computed Tomography is shown to be a quantitative and non-destructive technique for tracking fluid displacement process in cellulosic porous media. If immiscible displacement occurred with fluids having identical viscosities, the interface between the fluids was dispersed according to an idealized Fickian process. Using the method of moments we determined dispersion coefficients in all directions. It was confirmed that the dispersion coefficient was a linear function of the flow rate. These are consistent with the theoretical model of random walk in former paper.

ACKNOWLEDGEMENT

This work was supported (in part) by the Taegu University Research Grant, 1999.

NOMENCLATURE

A : unit area of porous bed [m^2]
D : dispersion coefficient [m^2/s]
l_p : length of a jump [m]
M : total number of capillaries [number]
$P^{(1)}(x, t)$: fractional concentration of microscopic interfaces between x and x+dx at time t [-]
Q : volumetric flow rate [m^3/s]
r_c : radius of a capillary [m]
t : time [s]
x : flow direction [m]
$x_{i,j}$: saturation fraction of displacing fluid which occupies the void space of voxel (i, j) [-]

Greek Letters

β : average displacement velocity at which all the interfaces move [m/s]
μ : linear attenuation coefficient [-]
μ_{water} : attenuation coefficient of water [-]
$\mu_{i,j}$: attenuation coefficient of a specific voxel (i, j) [-]
μ_1 : attenuation coefficient of displacing fluid [-]
μ_2 : attenuation coefficient of displaced fluid [-]
$\mu_{1,cellulose}$: attenuation coefficient of porous cellulose filled with displacing fluid in voxel (i, j) [-]
$\mu_{2,cellulose}$: attenuation coefficient of porous cellulose filled with displaced fluid in voxel (i, j) [-]
$\rho^{(1)}(x, t)$: the concentration of microscopic interface between x and x+dx at time t [number/m]
ϕ : porosity of the cellulosic porous bed [-]
$\phi_{i,j}$: the void fraction of the volume element (i, j) [-]
Φ_w : fluid saturation [-]

REFERENCES

Castellana, F. S., Spencer, J. L. and Cartolano, A., "Application of the Gamma Camera to Studies of Flow and Mixing in Reactor Vessels," *Ind. Eng. Chem. Fund.*, **19**, 222 (1980).

Chen, S., Qin, F., Kim, K.-H. and Watson, A.T., "NMR Imaging of Multiphase Flow in Porous Media," *AIChE J.*, **39**(6), 925 (1993).

Chuoke, R. L., Van Meurs, P. and Van der Poel, C., "The Instability of Slow, Immiscible, Viscous Liquid-Liquid Displacements in Permeable Media," *Trans. AIME*, **216**, 188 (1959).

Flannery, B. P., Deckman, H. W., Roberge, W. G. and Damico, K. L., "Three-Dimensional X-ray Microtomography," *Science*, **237**, 1439 (1987).

Huang, Y. B., "Gamma Camera Imaging of Oil Displacement in Porous Media and Its interpretation by Percolation Theory," Ph.D. Dissertation, Columbia University, New York (1986).

Kim, K.-H. and Chung, C.-H., "A Stochastic Analysis on the Flow of Two Immiscible Fluids in Porous Media: The Case when the Viscosities of the Fluids Are Equal," *Korean J. Chem. Eng.*, submitted (2001).

Leverette, M. C., "Flow of Oil-Water Mixtures through Unconsolidated Sands," *Trans. AIME*, **132**, 149 (1939).

Parson, R. W., "Microwave Alternation - A New Tool for Monitoring Saturation in Laboratory Flooding Experiments," *Soc. Pet. Eng. J.*, **15**, 302 (1975).

Paterson, L., "Diffusion-Limited Aggregation and Two-Fluid Displacements in Porous Media," *Phys. Rev. Lett.*, **52**(18), 1621 (1984).

Van Meurs, P., "The use of Transparent Three-Dimensional Models for Studying the Mechanisms of Flow Process in Oil Reservoirs," *Trans AIME*, **210**, 295 (1957).

Vinegar, H. J., "X-Ray CT and NMR Imaging of Rocks," *J. of Pet. Tech.*, **March**, 257 (1986).

Wang, S. Y., "Computer Assisted Tomography and Its Application in the Study of Multiphase Flow Through Porous Media," Ph.D. Dissertation, Columbia University, New York (1983).

Wang, S. Y., Ayral, S., Castellana, F. S. and Gryte, C. C., "Reconstruction of Oil Saturation Distribution Histories During Immiscible Liquid-Liquid Displacement by Computer-Assisted Tomography," *AIChE J.*, **30**, 642 (1984).

Wellington, S. L. and Vinegar, H. J., "CT Studies of Surfactant-Induced CO_2 Mobility Control," *SPE* #14393 (1985).

Willemsen, J. F., "Flow Through Porous Materials," Schlemberger-Doll Research Preprint (1983).